Biophysical Journal, Volume *111*

Supplemental Information

Antimicrobial Peptides Share a Common Interaction Driven by Membrane Line Tension Reduction

J. Michael Henderson, Alan J. Waring, Frances Separovic, and Ka Yee C. Lee

Experimental Methods

Peptide stocks

Peptide stocks at 1 mg/mL were generally prepared in a HEPES buffered saline (HBS) solution containing calcium (HBS+Ca: 10 mM HEPES, 150 mM NaCl, 2 mM Ca^{2+}, pH 7.5). Given alamethicin's larger hydrophobicity as compared to other AMPs, alamethicin was first serially diluted from 5 to 1 mg/mL using a 50% (v/v) aqueous methanol solution. Poor solubility of caerin-1.3 and kalata-B3 was observed and instead were dissolved in HBS+Ca containing 5% DMSO to obtain transparent stocks at 1 mg/mL. Peptide concentration was quantified by UV absorbance using a Hewlett-Packard 8453 UV/Vis spectrophotometer, with calculated absorption coefficients of 1520 (PG-1), 3840 (human β-defensin-1), 5120 (histatin-2), and 27,500 (indolicidin) mol^{-1} cm^{-1}, respectively, at 280 nm. The stock concentrations of chromophoric lacking peptides were instead determined by the mass dissolved in a given volume and later found to have less than a 5.5% error from the desired concentration, as quantified by amino acid analysis at the W. M. Keck Foundation Biotechnology Resource Laboratory, Yale University, New Haven, CT.

Preparation of large unilamellar vesicles

Large unilamellar vesicles (LUVs) were self-assembled via the freeze-thaw extrusion method (1). An aliquot of the dissolved lipid in chloroform was transferred to an acid-cleaned vial and a lipid film was formed on the glass walls with a stream of ultrahigh purity nitrogen gas (Airgas, Radnor Township, PA). The film was dried overnight under vacuum to ensure complete evaporation of the solvent. Ultrapure water was added to the dried lipid sample (achieving a typical concentration of 1 mg/mL) and multilamellar vesicles were formed by vigorous mechanical agitation for 1 hour at 40°C. After six freeze-thaw cycles, the lipid dispersion was extruded at least 21 times through polycarbonate membranes having a pore size of 100 nm (Avanti Polar Lipids, Alabaster, AL). The size distribution of the resulting LUVs was determined by dynamic light scattering (Zetasizer Nano-ZS, Malvern Instruments, Worcestershire, UK) and typically exhibited an average diameter of 130 ± 40 nm. LUVs were utilized within two weeks and stored in an incubator oven at 30°C to keep the vesicles above the main phase transition temperature for DMPC (T_m = 24°C).

Supported bilayer formation and atomic force microscopy

High grade mica (Ted Pella, Redding, CA) was fixed to a stainless steel specimen disc (Ted Pella, Redding, CA) and used as a solid substrate for supported phospholipid bilayer (SPB) formation. The mica was freshly cleaved and hydrated with a 10 mM $MgCl_2$ salt solution as divalent cations aid in the fusion of LUVs to negatively charged substrates (2, 3). Dilution of the LUV stock was made with the $MgCl_2$ solution to a concentration of 15 μg/mL, and 1 mL was injected into the imaging fluid cell. The solution was incubated for 3–5 minutes, during which bilayer patches self-assembled, covering approximately 20% of the mica surface in a given 20 x 20 μm^2 area. The superphase was exchanged for HBS+Ca to flush away un-fused vesicles.

Topographic images of the SPB patches were gathered in fluid at 30°C using a Cypher ES AFM (Asylum Research, Santa Barbara, CA) in tapping mode. Silicon-nitride cantilevers having a nominal spring constant of 0.25 N/m with sharpened silicon tips (Olympus BioLever Mini, BL-AC40TS, Asylum Research Probes, Santa Barbara, CA) were used and driven to a resonant

frequency (typically at 20 kHz) by blueDrive^{TM} photothermal excitation. The tips were decontaminated by UV-generated ozone before an experiment (PSD-UV Surface Decontamination System, Novascan, Ames, IA). Given cantilever variability, the chosen setpoint fell between 80 and 95% of the free amplitude in our experiments, which corresponded to a deflection of 20–25 nm, ensuring ample sample clearance. To prevent membrane damage and image artifacts, the drive amplitude was adjusted to achieve an attractive imaging regime that minimized forces during scanning. Micrographs were obtained at a scan rate of 3.0 Hz with a resolution of 512 pixels/line. Peptide aliquots were prepared in HBS+Ca and following injection were incubated for at least 15 min before continuing imaging. Assuming the bilayer coverage is $\sim$20% of the 1 cm^2 mica substrate, the number of moles of deposited DMPC lipids and that of peptide can be easily estimated to calculate a peptide-to-lipid (*P/L*) ratio. In the calculation, the area/molecule of DMPC was assumed to be 60 Å^2 (4) and a volume of 50 μL was used as a conservative estimate of the liquid droplet size based on the specifications of the Cypher ES AFM (www.asylumresearch.com).

Image processing and analysis

To improve image clarity, AFM scans were subjected to a first-order flattening procedure using the Asylum Research software implemented in IGOR Pro (WaveMetrics, Lake Oswego, OR) to compensate for sample tilt and offset between scan lines (raised features were excluded from the flattening algorithm). Similarly to Blanchette et al. (5), the bilayer shape factor, S, was calculated according to

$$S = P^2/4\pi A \tag{1}$$

to quantify membrane morphological changes as a result from AMP activity; here P is the perimeter and A is the surface area of the bilayer patch. Ideal circular morphologies will have a shape factor equal to 1, as derived from the perimeter and area equations for a circle. A given bilayer patch was selected by proper thresholding of the image to generate a mask, and then the perimeter length and surface area were calculated using the particle size analysis tool in Gwyddion (6). Any visible areas of mica substrate in perforated bilayers were excluded from the final mask, either through adjustment of the thresholding level and/or through the manual removal of mask pixels, so that the analysis was performed only on the membranes themselves. The bilayer height was analyzed from the distribution of surface heights over a scan (histogram analysis) or from a line section of a scan, depending on the quality of the image. As attractive mode imaging can artificially increase sample height profiles (7, 8) and lead to measurement variability between experiments, membrane height changes are reported as relative changes from the initial bilayer patch within an experiment.

Calcein Leakage Assay.

The extent of vesicle leakage induced by the interaction of alamethicin was assessed from the de-quenching of the water-soluble, membrane impermeable dye, calcein (9–11). Calcein was purchased from Sigma-Aldrich (St. Louis, MO) as a disodium salt powder and used without further purification. Calcein-loaded DMPC vesicles were prepared by the extrusion method as previously explained in a solution containing 60 mM calcein and 10 mM HEPES at pH 7.5. The osmolality of the dye solution was approximately 391 mOsm (5005 OSMETTE II, Precision Systems, Natick, MA). Un-trapped calcein was separated from the vesicle suspension by size exclusion

chromatography (Superdex 75, 10 x 300 mm column, GE Healthcare) using an isotonic eluent (10 mM HEPES, 205 mM NaCl, pH 7.5) that was within 1–2 mOsm of the internal dye solution of the vesicles, made by the adjustment of the salt concentration. To ensure the vesicle suspension remained above the main phase transition temperature for DMPC (T_m = 24°C), the sample loop, eluent, tubing, and the column were maintained at a temperature between 35°C–40°C during gel filtration. The total lipid concentration of the collected vesicle fraction was determined by a phosphorous assay (12–14). Dye-loaded DMPC vesicles were utilized immediately for fluorescence measurements as they tended to leak their entire contents within a 24 hour period following preparation.

A quartz cuvette with a 1 cm pathlength was filled with 3 mL of a 135 μg/mL solution of dye-loaded DMPC vesicles prepared in the isotonic buffer. Changes in the fluorescence intensity from the de-quenching of calcein were monitored at 515 nm at 30°C using a FluoroLog-3 spectrofluorometer (Horiba, Edison, NJ) with an excitation wavelength of 490 nm. The background fluorescence of the lipid sample alone, I_o, was obtained prior to the addition of peptide which defined the starting point, i.e. time zero, of the experiment. Serial dilutions were made from the 1 mg/mL alamethicin stock, as described in the main body of the text, using the isotonic buffer such that approximately 30–70 μL aliquots could be added to the cuvette to obtain the desired bulk concentration. However, the largest bulk concentration investigated, 50 μM alamethicin, required the addition of approximately 300 μL of the stock. The sample was gently stirred using a magnetic stir bar through the course of the measurement to ensure sample homogeneity. Finally, 100 μL of 10 % (v/v) Triton X-100 was added to each sample to completely solubilize the vesicles and release all the entrapped calcein to determine the maximal fluorescence, I_{max}. The fractional release of calcein at a given time point, F_t, was calculated according to

$$F_t = (I_t - I_o)/(I_{max} - I_o). \tag{2}$$

The kinetics of vesicle leakage in relation to antimicrobial peptide activity have been reasonably well described by multi-exponential functions (15–18). All leakage curves were fit in MATLAB (MathWorks Inc., Natick, MA) to a double-exponential decay model,

$$F_t = 1 - A_1 e^{-t \cdot k_1} - A_2 e^{-t \cdot k_2}, \tag{3}$$

where A_1 and $A_2 (\equiv 1 - A_1)$ are the amplitudes, and k_1 and k_2 are the respective rate constants of the individual exponential functions that describe two distinct processes leading to calcein leakage. Given that the overall leakage can be dominated by process 2 ($A_2 = 1$) in the limit when either A_1 or k_1 vanishes, process 2 can be attributed to pores whose probability to form increases with increasing peptide concentration. Therefore, process 1 refers to a graded-leakage mechanism as A_1 can only approach finite values below 1. A graded-leakage mechanism has been explained by the asymmetric insertion of peptides into the outer leaflet of the membrane which causes transient defects to form that allow peptides to translocate across the membrane to establish a mass balance. These transient openings lead to a graded mechanism of dye leakage that has been observed with several other AMPs (17, 19–21). The apparent leakage rate, k_{app}, was calculated by an amplitude-weighted average according to

$$k_{app} = A_1 k_1 + (1 - A_1) k_2, \tag{4}$$

as was similarly done by Gregory et al. (19, 20).

Dynamic Light Scattering

To ascertain the effect that alamethicin has on the integrity of the vesicles, changes in the size distribution of the dye-loaded DMPC LUVs was monitored by dynamic light scattering (Zetasizer Nano-ZS, Malvern Instruments, Worcestershire, UK). Briefly, 3 mL of a 135 μg/mL solution of dye-loaded DMPC vesicles was prepared as described above to which an appropriate amount of alamethicin was added to reach a desired bulk concentration. Approximately 1 mL of the mixed DMPC-alamethicin solution was added to fill a capillary cell for measurement. DLS measurements were performed at 30°C and the sample was illuminated with 633 nm light provided from a He-Ne laser. The scattered light from the sample was analyzed at an angle of 173° from the incident beam in the backscattering configuration. Correlation analysis gave the diffusion coefficients of the vesicles from which the diameters of the LUVs were calculated using the Stokes-Einstein relationship. Scattering data were gathered over 15 minutes in which 12 individual measurements were combined to generate a single run. Reproducibility was assessed across 3 separate runs and averaged.

Table S1: Characteristics of the investigated AMPs.

Peptide	Charge at pH 7.5	No. of Residues	Sequence
Dermcidin	-3	48	SSLLEKGLDGAKKAVGGLGKLGKDAVEDLESVGK-GAVHDVKDVLDSVL
Kalata-B3	-2	30	GLPTCGETCFGGTCNTPGCTCDPWPICTRD
Caerin-1.3	0	25	GLLSVLGSVAQHVLPHVVPVIAEHL - NH_2
Alamethicin	0	20	Ac-UPUAUAQUVUGLUPVUUQQ-Phl
Pardaxin-1	0	33	GFFALIPKIISSPLFKTLLSAVGSALSSSGEQE
Histatin-2	0	27	RKFHEKHHSHREFPFYGDYGSNYLYDN
Aurein-1.1	+1	13	GLFDIIKKIAESI - NH_2
Citropin-1.1	+2	16	GLFDVIKKVASVIGGL - NH_2
Magainin-1	+3	23	GIGKFLHSAGKFGKAFVGEIMKS
Dermaseptin-1	+3	34	ALWKTMLKKLGTMALHAGKAALGAAADTISQGTQ
Indolicidin	+4	13	ILPWKWPWWPWRR - NH_2
Human β-Defensin-1	+4	36	DHYNCVSSGGQCLYSACPIFTKIQGTCYRGKAKCCK
Protegrin-1	+7	18	RGGRLCYCRRRFCVCVGR - NH_2

The terminal protecting group abbreviations are Ac- for acetyl and NH_2 for carboxyamide. The following abbreviations are used for non-standard residues: U, α-aminoisobutyric acid; Phl, L-phenylalaninol. Solid lines indicate residue connections in cyclic structures while disulfide bonds between cysteine residues are indicated by dashed lines.

Table S2: Minimum inhibitory concentrations, MIC (μM), of the investigated AMPs or related isoforms against susceptible Gram-negative and Gram-positive bacterial strains.

	Gram -		Gram +		
Peptide	*E. coli*	*P. aeruginosa*	*S. aureus*	*B. subtilis*	Ref.
Dermcidin	0.21[a]	?	0.21[a]	?	(22)
Kalata-B1*	>500	>500	>500	?	(23)
Caerin-1.1*	100–200[a,b]	?	3[a]	12[a]	(24)
Alamethicin	8–102[a,c]	?	18[a]	8	(25–27)
Pardaxin-1	13	25	?	?	(28)
Aurein-1.2*	75	?	35[a]	?	(29, 30)
Citropin-1.1	40–79[a,b]	?	8[a]	2[a]	(24)
Magainin-2*	0.1–2[a,d]	0.8–52[a,d]	2–52[a,d]	?	(31)
Dermaseptin-1	12	?	12	?	(32)
Indolicidin	0.3–4[a,d]	4–67[a,d]	2–17[a,d]	?	(31)
Protegrin-1	0.35[a]	0.23[a]	0.79[a]	6[a]	(33, 34)

? MIC value could not be found.

* Related isoform that differs by one amino acid residue to the investigated peptide in Table S1.

[a] MIC value(s) converted from results reported in μg/mL.

[b] Reported range from two strains.

[c] Reported range from two peptide isoforms.

[d] Reported range from 30 clinical isolates.

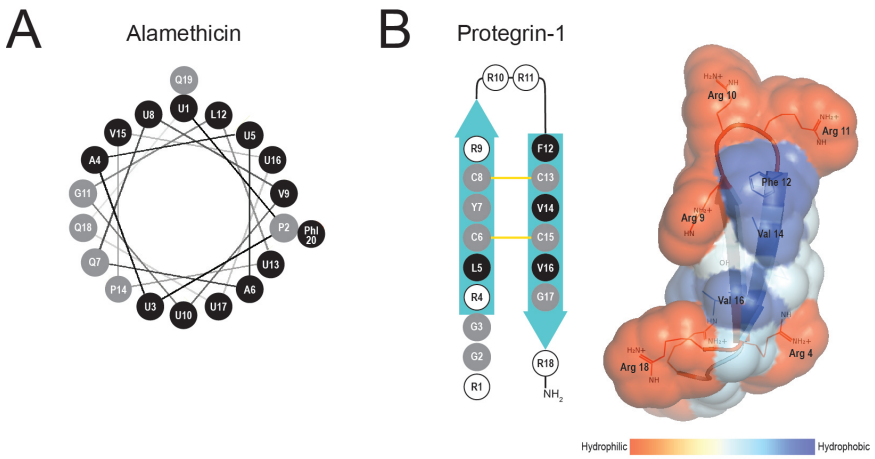

Figure S1: Secondary structure representation of alamethicin (A) and protegrin-1 (B). In the helical wheel diagram of alamethicin, α-aminoisobutyric acid and L-phenylalaninol are abbreviated with U and Phl, respectively. The hydrophobicity of protegrin-1 (PDB ID: 1PG1) was rendered as a colored surface in PyMOL based on the Kyte-Doolittle scale (35), where the gradation of color from red to blue signifies a transition from more to less hydrophilic. Residues in the primary sequences were color-coded according to the following scheme: black, apolar; gray, polar un-charged; and white, charged. Disulfide bonds are represented as yellow lines between connected cysteine residues.

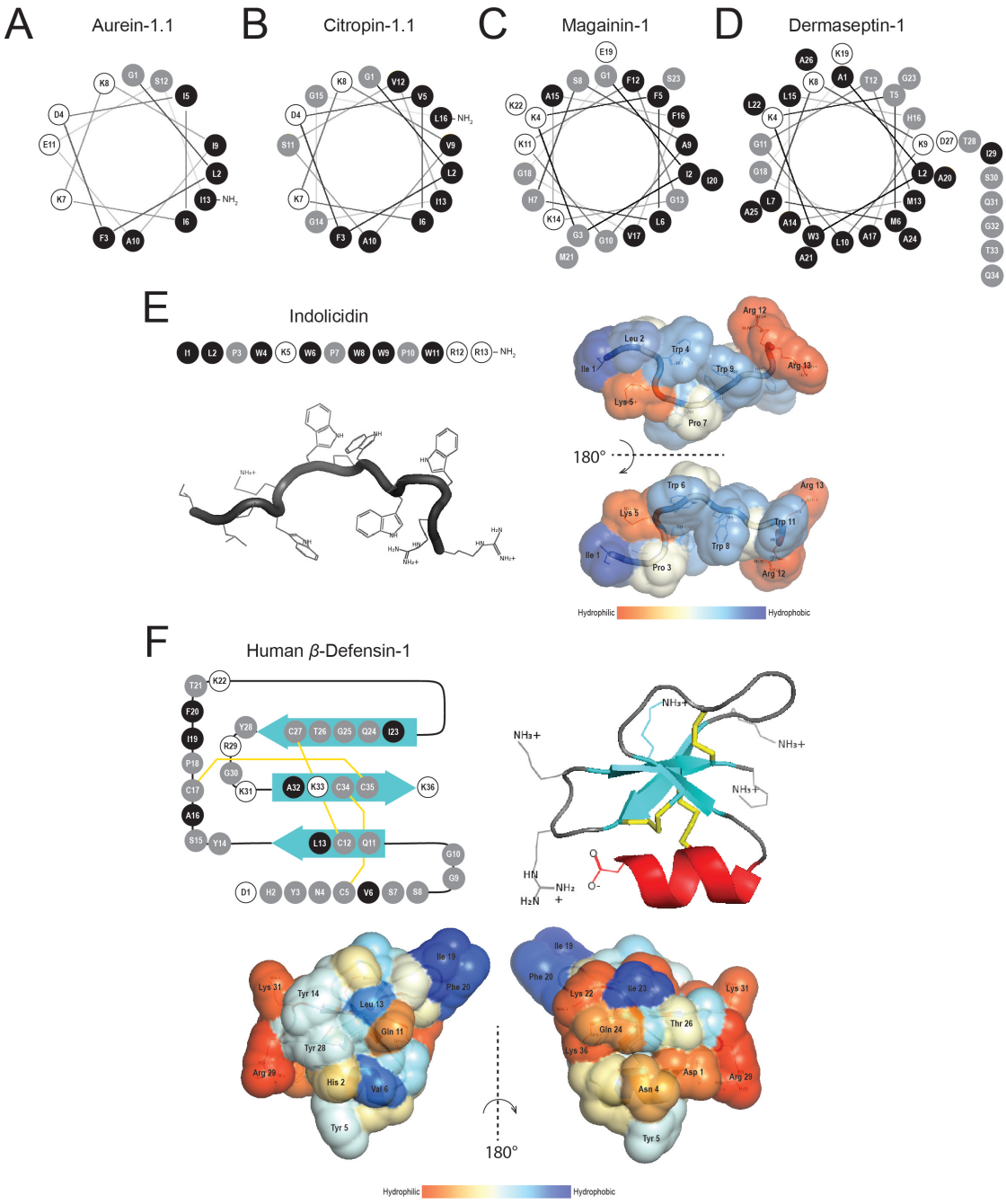

Figure S2: Secondary structure representations of the positively charged AMPs, aurein-1.1 (A), citropin-1.1 (B), magainin-1 (C), dermaseptin-1 (D), indolicidin (E), and human β-defensin-1 (F), featured in Fig. 3 of the main text. Structural renderings of indolicidin (PDB ID: IG8C) and β-defensin-1 (PDB ID: 1IJV) were done in PyMOL and their hydrophobicity was rendered as a colored surface based on the Kyte-Doolittle scale (35) where the gradation of color from red to blue signifies a transition from more to less hydrophilic. Residues in the primary sequences were color-coded according to the following scheme: black, apolar; gray, polar un-charged; and white, charged. Disulfide bonds are represented as yellow lines between connected cysteine residues.

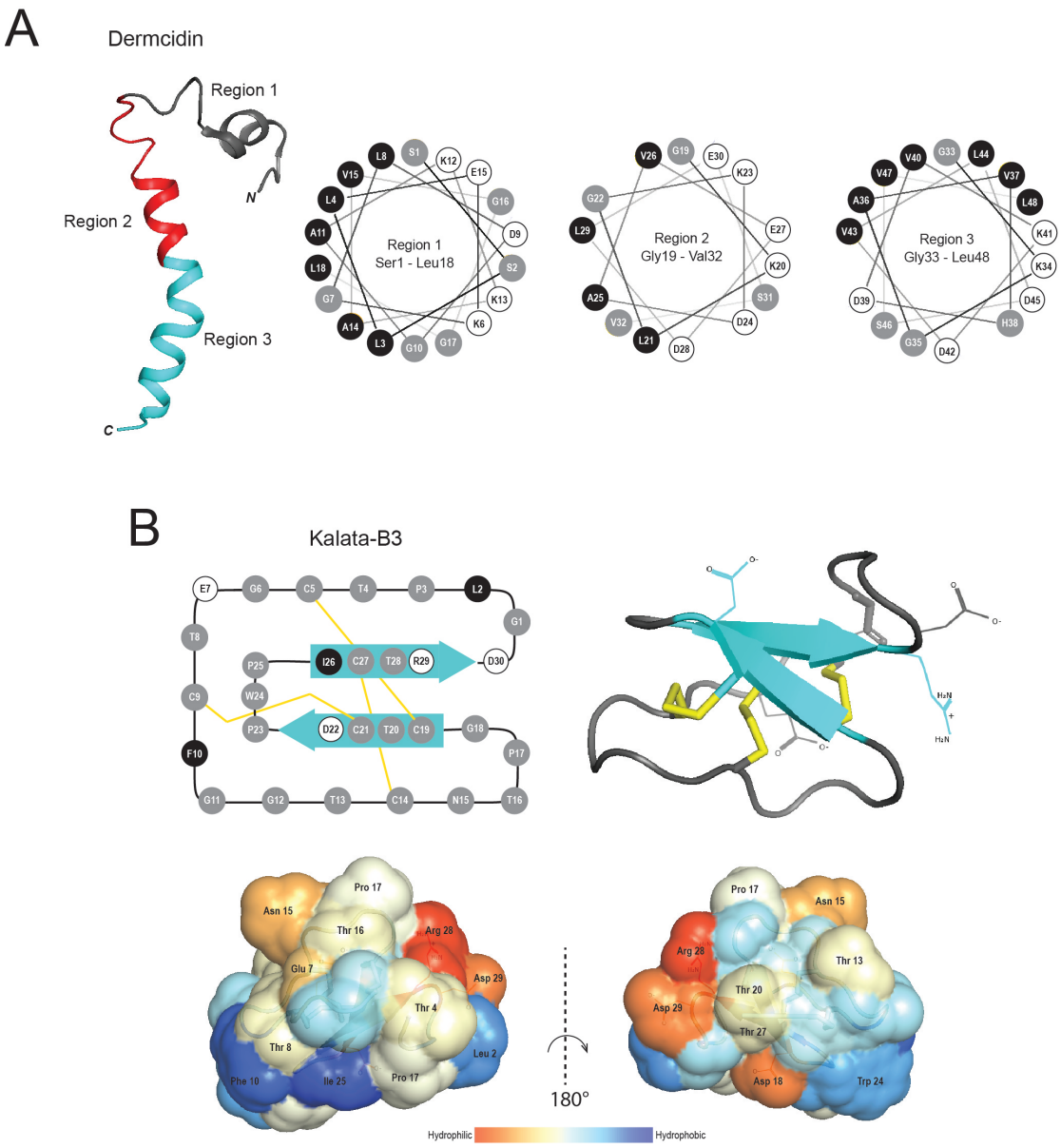

Figure S3: Secondary structure representations of the negatively charged AMPs, dermcidin (A) and kalata-B3 (B), featured in Fig. 4 of the main text. (A) The secondary structure of dermcidin (PDB ID: 2KSG) was rendered in PyMOL to display its flexible helix-hinge-helix type motif consisting of three amphiphilic helices colored black (region 1, Ser1–Leu18), red (region 2, Gly19–Val32), and cyan (region 3, Gly33–Leu48). Helical wheel diagrams were constructed for each region in order to show that an overall amphipathic structure can be formed when the helices are properly oriented with respect to one another. (B) Since no PDB file could be obtained for the cyclotide kalata-B3, we instead rendered kalata-B1 (PDB ID: 1ZNU) in PyMOL as it only differed from kalata-B3 by a lack of a single proline found in the C-terminal end. The hydrophobicity of kalata was rendered as a colored surface based on the Kyte-Doolittle scale (35), where the gradation of color from red to blue signifies a transition from more to less hydrophilic. Residues in the primary sequences were color-coded according to the following scheme: black, apolar; gray, polar un-charged; and white, charged. Disulfide bonds are represented as yellow lines between connected cysteine residues.

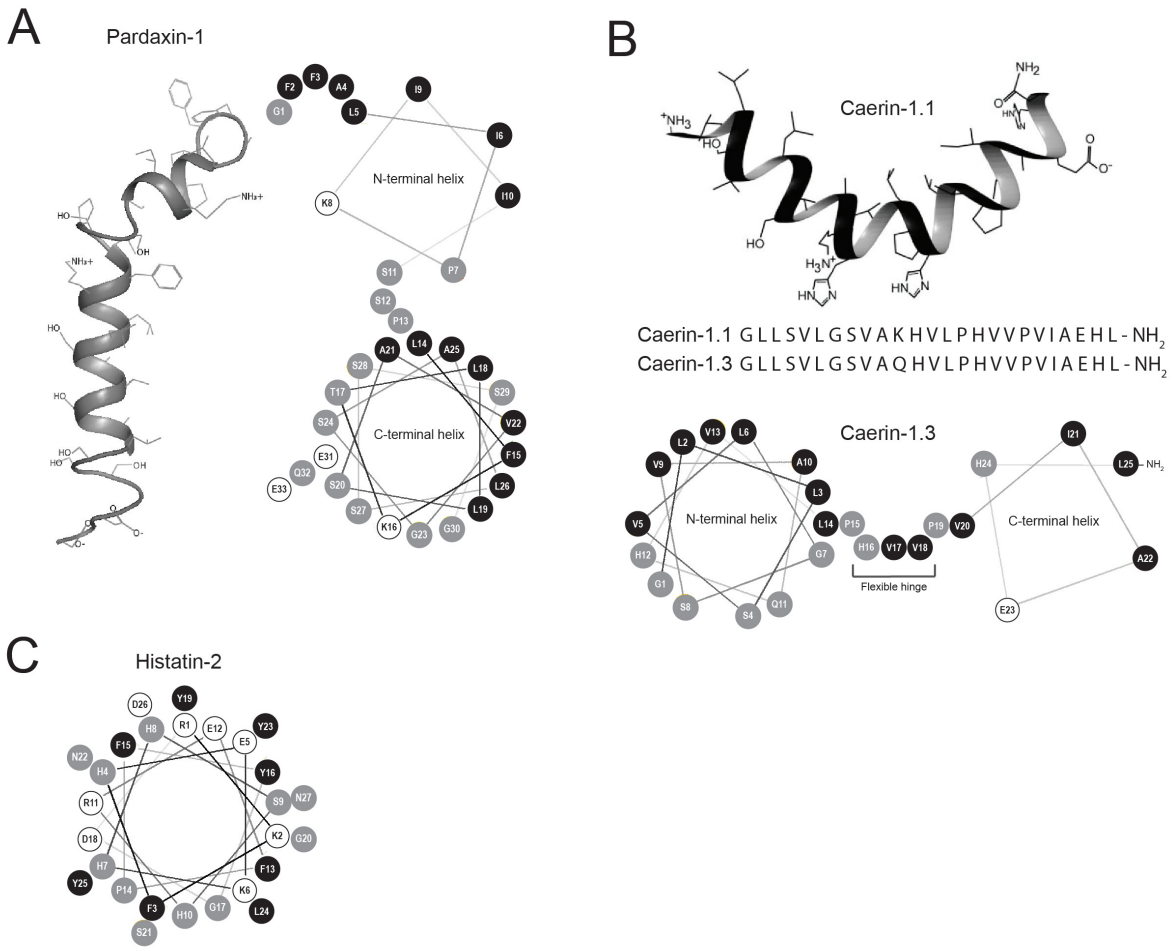

Figure S4: Secondary structure representations and helical wheel diagrams of the neutral AMPs, pardaxin-1 (A), caerin-1.3 (B), and histatin-2 (C), featured in Fig. 5 of the main text. (A) Since no PDB file was present for pardaxin-1, the helical structure of pardaxin-Pa4 (PDB ID: 1XC0) was used as a template with which Gly31 was mutated to a Glu to make the primary sequence identical to that of pardaxin-1. (B) As no PDB file could be found of a caerin peptide in the database, the helical structure depicted in B is that of caerin-1.1 (reprinted from (36)), a homolog of caerin-1.3 that differs by only one residue. (C) While limited structural information exists for histatin peptides, the helical wheel generated for histatin-2 shows no clear segregation of hydrophilic and hydrophobic residues that form an ideal amphipathic secondary structure. Residues in the primary sequences were color-coded according to the following scheme: black, apolar; gray, polar un-charged; and white, charged.

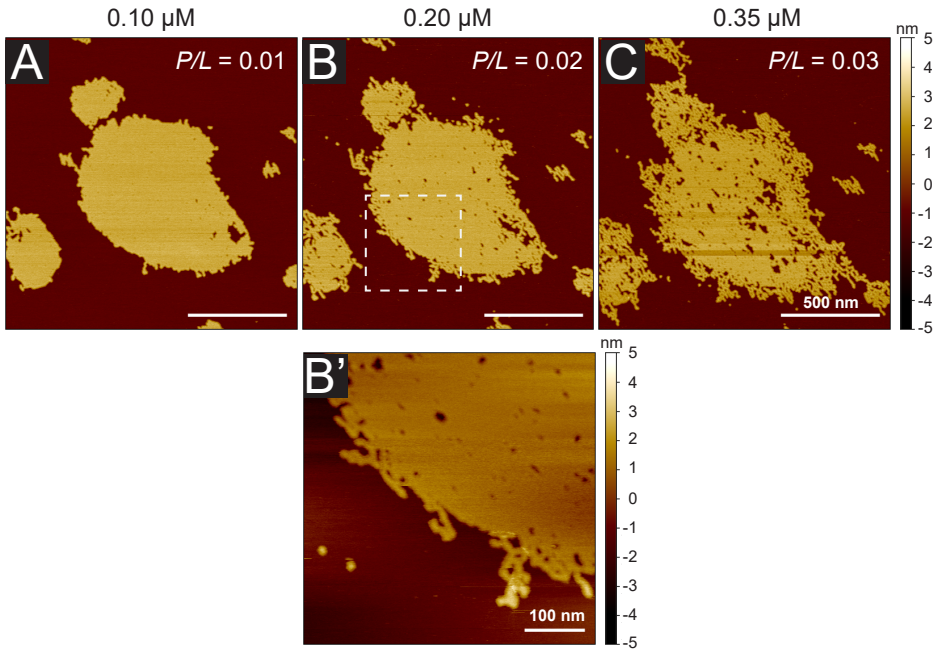

Figure S5: Membrane structural transformations induced by PG-1. The formation of porous defects within the bilayer core was observed at 0.10 μM PG-1 (A) which increased in number and size in the range of 0.20 to 0.35 μM PG-1 (B and C). The dashed box in B indicates a zoomed in region (500 x 500 nm^2) that is shown in B'. All images were gathered at 30°C. White scale bars are 500 nm, unless otherwise indicated.

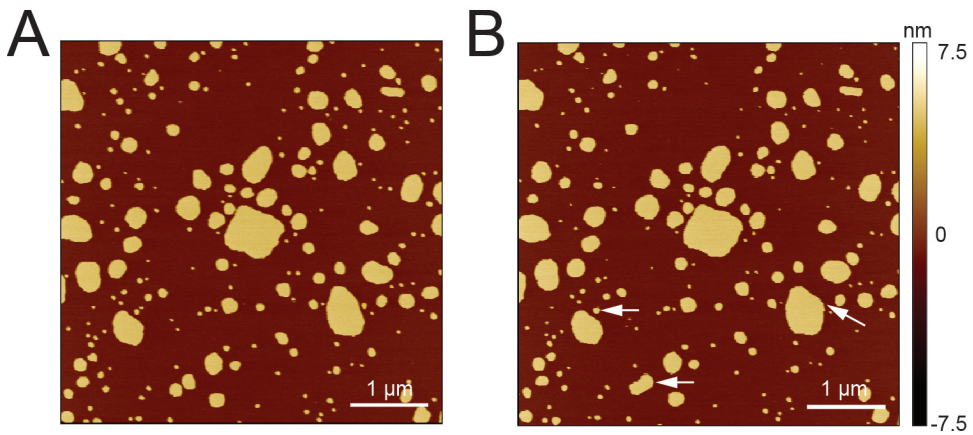

Figure S6: DMPC bilayers imaged under different buffered superphase conditions. (A) Prior to the introduction of alamethicin (see Fig. 2 main text), the same DMPC bilayers were imaged first in the HBS+Ca buffer (10 mM HEPES, 150 mM NaCl, 2 mM Ca^{2+}, pH 7.5) alone. (B) The superphase was then exchanged with a HBS+Ca solution containing 2% DMSO and 4% MeOH (v/v) to mimic that of a 50 μM alamethicin injection. Negligible changes between (A) and (B) were observed and only three events of adjacent bilayer fusion were seen (white arrows) within the 5 x 5 μm^2 viewing area. Images were gathered at 30°C. White scale bars are 1 μm.

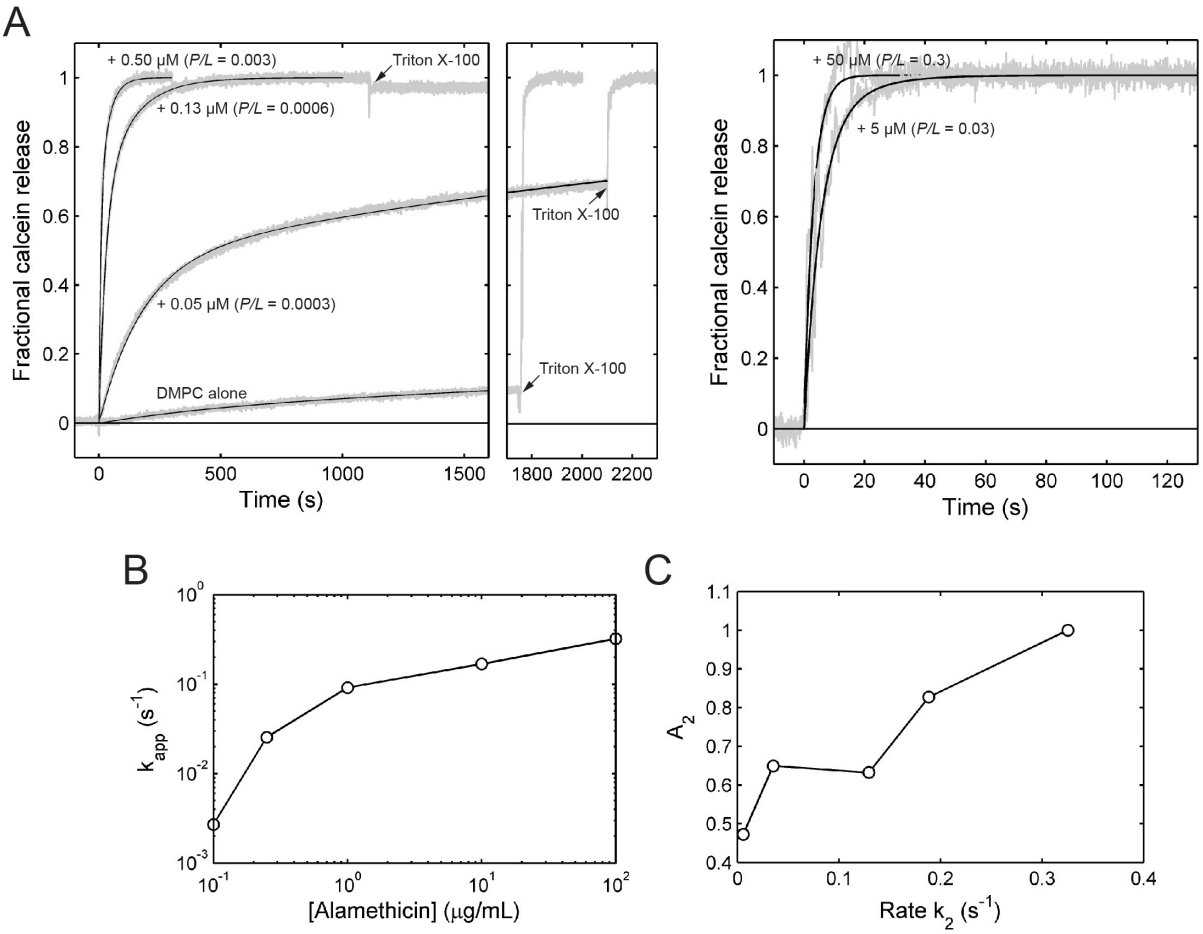

Figure S7: Concentration-dependent leakage of entrapped calcein in DMPC LUVs by alamethicin. For all experiments the total lipid concentration was held constant at 135 μg/mL and the experimental temperature was maintained at 30°C. (A) Higher bulk concentrations of alamethicin resulted in progressively higher plateaus in the maximum fraction of released calcein in the leakage profiles. Complete leakage was eventually obtained at a bulk alamethicin concentration of 0.13 μM and higher. Detergent addition to these samples would slightly dilute the free calcein by roughly 5% from a lowering of the fluorescence intensity; consequently, all the calcein had been released from the addition of alamethicin prior to the Triton X-100 addition. (B) As evident in the leakage profiles presented in A, the apparent rate of leakage, k_{app}, steadily increased with increasing alamethicin concentration, signifying more membrane-bound alamethicin to perturb the integrity of the calcein-loaded vesicles. (C) The resulting parameters A_2 and k_2 from the double-exponential fit to the leakage profiles were correlated to each other. As the bulk concentration of alamethicin was increased, the leakage process corresponding to stable pore formation (process 2 with amplitude A_2) had a greater contribution (i.e., a greater weight or amplitude) to the overall leakage profile with a higher density of pores from the increase in k_2.

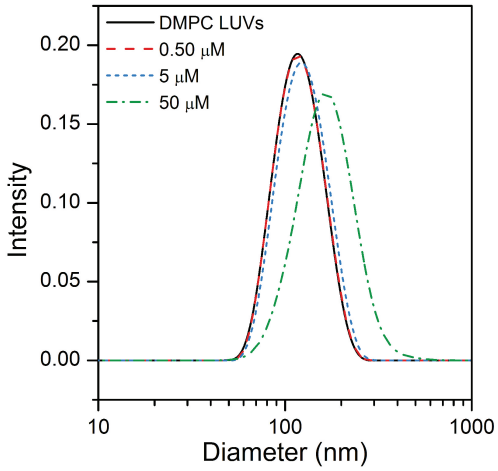

Sample	Average size (± s.d.)
DMPC LUVs	122.1 ± 32.9 nm
DMPC + 0.50 μM alamethicin (*P/L* = 0.003)	122.5 ± 32.9 nm
DMPC + 5.0 μM alamethicin (*P/L* = 0.03)	128.2 ± 35.5 nm
DMPC + 50 μM alamethicin (*P/L* = 0.3)	173.0 ± 56.9 nm

Figure S8: DLS analysis of DMPC LUV size distribution changes at 30°C with increasing bulk concentrations of alamethicin.

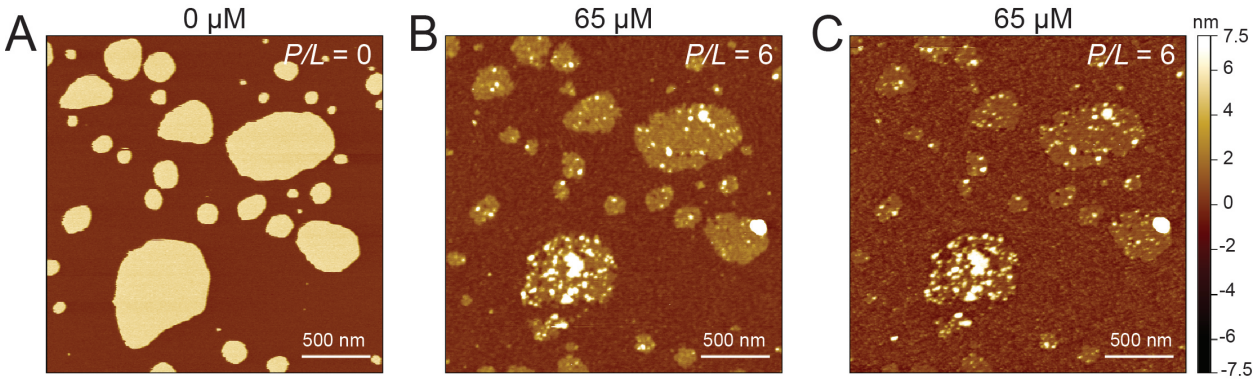

Figure S9: Time lapse imaging of kalata-B3's slow solubilization of zwitterionic DMPC bilayers. (A) DMPC bilayer patches in the absence of peptide. (B) Image collected 15 min following the addition of a 65 μM aliquot of kalata-B3. (C) Image collected 1 hour later after B. All images were gathered at 30°C. White scale bars are 500 nm.

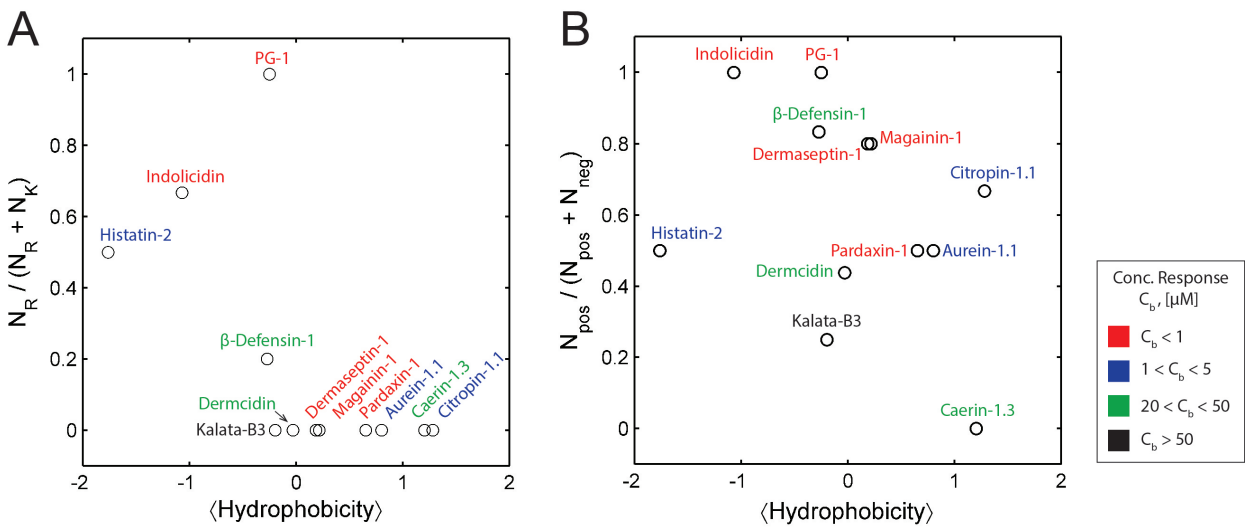

Figure S10: Amino acid content comparison of the investigated line-active peptides. (A) The ratio of the number of arginines to the number of arginines + number of lysines ($N_R/(N_R+N_K)$) plotted against their average hydrophobicity (Kyte-Doolittle scale). (B) The ratio of the number of positive residues (arginines + lysines) to the total number of charged residues (positive + negative), ($N_{pos}/(N_{pos}+N_{neg})$), plotted against the average hydrophobicity (Kyte-Doolittle scale) calculated for each peptide. The peptides were color-coded based upon their concentration response (C_b) in achieving a final micellized state.

References

1. Muresan, A. S., and K. Y. C. Lee. 2001. Shape evolution of lipid bilayer patches adsorbed on mica: an atomic force microscopy study. *J. Phys. Chem. B.* 105:852–855.
2. Reviakine, I., and A. Brisson. 2000. Formation of supported phospholipid bilayers from unilamellar vesicles investigated by atomic force microscopy. *Langmuir.* 16:1806–1815.
3. Seantier, B., and B. Kasemo. 2009. Influence of mono- and divalent ions on the formation of supported phospholipid bilayers via vesicle adsorption. *Langmuir.* 25:5767–5772.
4. Kučerka, N., Y. Liu, N. Chu, H. I. Petrache, S. Tristram-Nagle, and J. F. Nagle. 2005. Structure of fully hydrated fluid phase DMPC and DLPC lipid bilayers using x-ray scattering from oriented multilamellar arrays and from unilamellar vesicles. *Biophys. J.* 88:2626–2637.
5. Blanchette, C. D., C. A. Orme, T. V. Ratto, and M. L. Longo. 2007. Quantifying growth of symmetric and asymmetric lipid bilayer domains. *Langmuir.* 24:1219–1224.
6. Nečas, D., and P. Klapetek. 2012. Gwyddion: an open-source software for SPM data analysis. *Cent. Eur. J. Phys.* 10:181–188.
7. R. Brandsch, G. B., and, and M.-H. Whangbo. 1997. On the factors affecting the contrast of height and phase images in tapping mode atomic force microscopy. *Langmuir.* 13:6349–6353.
8. San Paulo, A., and R. García. 2000. High-resolution imaging of antibodies by tapping-mode atomic force microscopy: attractive and repulsive tip-sample interaction regimes. *Biophys. J.* 78:1599–1605.
9. Allen, T. M., and L. G. Cleland. 1980. Serum-induced leakage of liposome contents. *BBA - Biomembranes.* 597:418 – 426.
10. Matsuzaki, K., M. Harada, T. Handa, S. Funakoshi, N. Fujii, H. Yajima, and K. Miyajima. 1989. Magainin 1-induced leakage of entrapped calcein out of negatively-charged lipid vesicles. *BBA - Biomembranes.* 981:130–134.
11. Pouny, Y., D. Rapaport, A. Mor, P. Nicolas, and Y. Shai. 1992. Interaction of antimicrobial dermaseptin and its fluorescently labeled analogs with phospholipid membranes. *Biochemistry.* 31:12416–12423.
12. Chen, P. S., T. Y. Toribara, and H. Warner. 1956. Microdetermination of phosphorus. *Anal. Chem.* 28:1756–1758.
13. Bartlett, G. R.. 1959. Phosphorus assay in column chromatography. *J. Biol. Chem.* 234:466–468.
14. Morrison, W.. 1964. A fast, simple and reliable method for the microdetermination of phosphorus in biological materials. *Anal. Biochem.* 7:218 – 224.
15. Arbuzova, A., and G. Schwarz. 1996. Pore kinetics of mastoparan peptides in large unilamellar lipid vesicles. *Progr. Colloid Polym. Sci.* 100:345–350.
16. Rex, S., and G. Schwarz. 1998. Quantitative studies on the melittin-induced leakage mechanism of lipid vesicles. *Biochemistry.* 37:2336–2345.
17. Heerklotz, H., and J. Seelig. 2007. Leakage and lysis of lipid membranes induced by the lipopeptide surfactin. *Euro. Biophys. J.* 36:305–314.
18. Andersson, A., J. Danielsson, A. Gräslund, and L. Mäler. 2007. Kinetic models for peptide-induced leakage from vesicles and cells. *Euro. Biophys. J.* 36:621–635.
19. Gregory, S. M., A. Cavenaugh, V. Journigan, A. Pokorny, and P. F. Almeida. 2008. A quantitative model for the all-or-none permeabilization of phospholipid vesicles by the antimicrobial peptide cecropin A. *Biophys. J.* 94:1667–1680.

20. Gregory, S. M., A. Pokorny, and P. F. Almeida. 2009. Magainin 2 revisited: a test of the quantitative model for the all-or-none permeabilization of phospholipid vesicles. *Biophys. J.* 96:116–131.
21. Heerklotz, H.. 2001. Membrane stress and permeabilization induced by asymmetric incorporation of compounds. *Biophys. J.* 81:184–195.
22. Schittek, B., R. Hipfel, B. Sauer, J. Bauer, H. Kalbacher, S. Stevanovic, M. Schirle, K. Schroeder, N. Blin, F. Meier, G. Rassner, and C. Garbe. 2001. Dermcidin: a novel human antibiotic peptide secreted by sweat glands. *Nat. Immunol.* 2:1133–1137.
23. Tam, J. P., Y.-A. Lu, J.-L. Yang, and K.-W. Chiu. 1999. An unusual structural motif of antimicrobial peptides containing end-to-end macrocycle and cystine-knot disulfides. *Proc. Natl. Acad. Sci. U.S.A.* 96:8913–8918.
24. Brian Chia, C. S., Y. Gong, J. H. Bowie, J. Zuegg, and M. A. Cooper. 2011. Membrane binding and perturbation studies of the antimicrobial peptides caerin, citropin, and maculatin. *Biopolymers.* 96:147–157.
25. Wenschuh, H., M. Beyermann, H. Haber, J. K. Seydel, E. Krause, and M. Bienert. 1995. Stepwise automated solid phase synthesis of naturally occurring peptaibols using FMOC amino acid fluorides. *J. Org. Chem.* 60:405–410.
26. Ayers, S., B. M. Ehrmann, A. F. Adcock, D. J. Kroll, E. J. Carcache de Blanco, Q. Shen, S. M. Swanson, J. O. Falkinham III, M. C. Wani, S. M. Mitchell, C. J. Pearce, and N. H. Oberlies. 2012. Peptaibols from two unidentified fungi of the order Hypocreales with cytotoxic, antibiotic, and anthelmintic activities. *J. Pept. Sci.* 18:500–510.
27. Barns, K. J., and J. C. Weisshaar. 2016. Single-cell, time-resolved study of the effects of the antimicrobial peptide alamethicin on *Bacillus subtilis*. *BBA-Biomembranes.* 1858:725–732.
28. Oren, Z., and Y. Shai. 1996. A class of highly potent antibacterial peptides derived from pardaxin, a pore-forming peptide isolated from Moses sole fish *Pardachirus marmoratus*. *Eur. J. Biochem.* 237:303–310.
29. Li, X., Y. Li, A. Peterkofsky, and G. Wang. 2006. NMR studies of aurein 1.2 analogs. *BBA-Biomembranes.* 1758:1203–1214.
30. Rozek, T., K. L. Wegener, J. H. Bowie, I. N. Olver, J. A. Carver, J. C. Wallace, and M. J. Tyler. 2000. The antibiotic and anticancer active aurein peptides from the Australian Bell Frogs *Litoria aurea* and *Litoria raniformis*. *Eur. J. Biochem.* 267:5330–5341.
31. Giacometti, A., O. Cirioni, F. Barchiesi, M. S. Del Prete, M. Fortuna, F. Caselli, and G. Scalise. 2000. In vitro susceptibility tests for cationic peptides: comparison of broth microdilution methods for bacteria that grow aerobically. *Antimicrob. Agents Chemother.* 44:1694–1696.
32. Savoia, D., R. Guerrini, E. Marzola, and S. Salvadori. 2008. Synthesis and antimicrobial activity of dermaseptin S1 analogues. *Bioorg. Med.* 16:8205–8209.
33. Steinberg, D. A., M. A. Hurst, C. A. Fujii, A. H. C. Kung, J. F. Ho, F. Cheng, D. J. Loury, and J. C. Fiddes. 1997. Protegrin-1: a broad-spectrum, rapidly microbicidal peptide with in vivo activity. *Antimicrob. Agents Chemother.* 41:1738–1742.
34. Lai, J. R., R. F. Epand, B. Weisblum, R. M. Epand, and S. H. Gellman. 2006. Roles of salt and conformation in the biological and physicochemical behavior of protegrin-1 and designed analogues: correlation of antimicrobial, hemolytic, and lipid bilayer-perturbing activities. *Biochemistry.* 45:15718–15730.
35. Kyte, J., and R. F. Doolittle. 1982. A simple method for displaying the hydropathic character of a protein. *J. Mol. Biol.* 157:105–132.

36. Pukala, T. L., J. H. Bowie, V. M. Maselli, I. F. Musgrave, and M. J. Tyler. 2006. Host-defence peptides from the glandular secretions of amphibians: structure and activity. *Nat. Prod. Rep.* 23:368–393.